Anisotropic In-Plane Resistivity in the Nematic Phase of the Iron Pnictides

Rafael M. Fernandes, Elihu Abrahams, and Jörg Schmalian

Phys. Rev. Lett. **107**, 217002 — Published 14 November 2011

DOI: 10.1103/PhysRevLett.107.217002

Anisotropic in-plane resistivity in the nematic phase of the iron pnictides

Rafael M. Fernandes,[1,*] Elihu Abrahams,[2] and Jörg Schmalian[1,†]

[1] *Ames Laboratory and Department of Physics and Astronomy, Iowa State Univ., Ames, IA 50011, USA*
[2] *Department of Physics and Astronomy, University of California Los Angeles, Los Angeles, CA 90095, USA*

We show that the interference between scattering by impurities and by critical spin fluctuations gives rise to anisotropic transport in the Ising-nematic state of the iron pnictides. The effect is closely related to the non-Fermi liquid behavior of the resistivity near an antiferromagnetic quantum critical point. Our theory not only explains the observed sign of the resistivity anisotropy $\Delta\rho$ in electron doped systems, but also predicts a sign change of $\Delta\rho$ upon sufficient hole doping. Furthermore, our model naturally addresses the changes in $\Delta\rho$ upon sample annealing and alkaline-earth substitution.

In many materials, anisotropic properties are related to the underlying crystalline structure. However, when correlations are present, the electronic states can themselves become anisotropic [1]. Recent transport measurements in detwinned crystals of the iron pnictide compounds $AE\mathrm{Fe_2As_2}$ (AE = Ba, Ca, Sr) found an in-plane anisotropy that cannot be attributed only to lattice distortions, unveiling an anisotropic electronic state [2, 3]. Its existence is also supported by the observations of an orbital polarization $\mathcal{O} = n_{xz} - n_{yz}$ of d_{xz} and d_{yz} Fe states in angle-resolved photoemission spectroscopy (ARPES) [4], local anisotropies in scanning tunneling microscopy [5], and anisotropies in the optical spectrum [6–8].

One candidate for such unconventional electronic state is the Ising-nematic order, which emerges from the combination of magnetic fluctuations and frustration [9–13]. In a strong-coupling approach, frustration is promoted by the competing $J_1 - J_2$ exchange interactions, while in an weak-coupling approach, it follows from the degeneracy of the magnetic ground state due to the nesting properties of the Fermi surface (FS). Indeed, the iron pnictides support two magnetic instabilities with order parameters $\mathbf{\Delta}_1$, $\mathbf{\Delta}_2$ corresponding to the in-plane ordering vectors $\mathbf{Q}_1 = (\pi, 0)$, $\mathbf{Q}_2 = (0, \pi)$, respectively. The electronic structure [14, 15], as well as the coupling to the lattice [13], give rise to the coupling $g\Delta_1^2\Delta_2^2$ in the free energy, with $g > 0$. As a result, a discrete Ising-nematic degree of freedom $\varphi \propto \langle\Delta_1^2\rangle - \langle\Delta_2^2\rangle$ emerges, which labels the two degenerate states $\Delta_1 \neq 0$, $\Delta_2 = 0$ and $\Delta_1 = 0$, $\Delta_2 \neq 0$. Most importantly, φ is able to order at a temperature T_s above the onset of antiferromagnetism (AFM) at T_N [16], breaking the tetragonal symmetry already in the paramagnetic (PM) phase - hence the term nematic.

By symmetry, Ising-nematic order induces the orbital polarization $\mathcal{O}$ and a shear distortion ε_s, driving a structural transition from the tetragonal (Tet) to the orthorhombic (Ort) phase at T_s. It explains why T_s and T_N track each other closely across every pnictide phase diagram, even inside the superconducting (SC) dome [17, 18]. Recently, it has been shown that nematic fluctuations can explain the dramatic softening of the lattice observed experimentally in the Tet phase [13]. It remains an important issue whether this scenario is also able to address the observed in-plane resistivity anisotropy $\Delta\rho \equiv \rho_b - \rho_a$, where b (a) refers to the direction with shorter (longer) lattice constant of the Ort state. The induced orbital polarization $\mathcal{O}$ has been alternatively proposed to explain such anisotropy, but different authors disagree on the suitability of this proposal [19, 20].

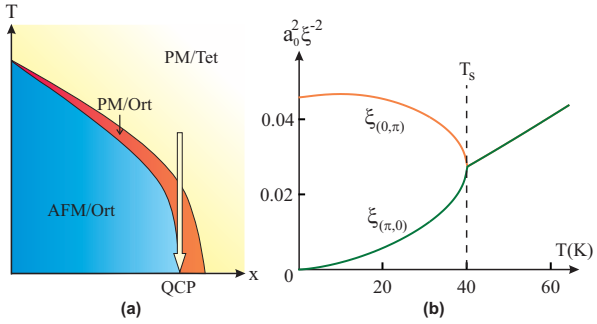

Figure 1: **(a)** Schematic temperature-doping (T, x) phase diagram in the absence of SC. The yellow region corresponds to enhanced nematic fluctuations, as seen by elastic modulus measurements [13]. **(b)** Temperature dependence of the correlation lengths ξ associated with the $(\pi, 0)$ and $(0, \pi)$ magnetic instabilities above the magnetic QCP.

In this paper we demonstrate that the observed anisotropic transport *above* T_N can be understood within the Ising-nematic picture. Our model explains in a unified way several experimental observations, such as the sign of the anisotropy [2, 3] and the changes in $\Delta\rho$ upon sample annealing [8] or alkaline-earth substitution [21]. We also predict a sign change of $\Delta\rho$ for hole-doped systems, thus addressing the peculiar observations in K-doped compounds [22, 23]. Our results support the view that nematic order is the driving force for the structural transition and the orbital polarization in the pnictides. Note that our theory does not address the anisotropy observed *below* T_N, in the AFM state. However, in all observations, the sign of $\Delta\rho$ is already set above T_N, where the slope $d(\Delta\rho)/dT$ is the largest [2, 3]. Concentrating on the regime above T_N allows for a more transparent and less model-dependent understanding of the resistivity anisotropy.

Below T_s, the onset of a finite Ising-nematic order pa-

rameter $\varphi \neq 0$ gives rise to two sources of anisotropy: in the electronic structure itself and in the spectrum of magnetic fluctuations. The former is rather weak, due to the smallness of the shear distortion $\varepsilon_s = (a-b)/(a+b)$ - for instance, in optimally doped $Ba(Fe_{1-x}Co_x)_2As_2$, $\varepsilon_s \approx 5 \times 10^{-4}$ [4, 17]. On the other hand, the latter is strong, since only fluctuations associated with one of the magnetic instabilities diverge. The impact of this anisotropy on the transport depends on the contribution of the scattering of electrons by spin fluctuations around the hot spots of the Fermi surface, defined via $\varepsilon_{\lambda,\mathbf{k}} = \varepsilon_{\lambda',\mathbf{k}+\mathbf{Q}_i}$, with $\varepsilon_{\lambda,\mathbf{k}}$ denoting the dispersion of band λ. In ultra-clean systems, this scattering channel is short-circuited by the contribution from the other regions of the FS [24]. However, in the presence of significant impurity scattering, the scattering by spin fluctuations becomes important, leading to non-Fermi liquid behavior [25] and, in addition, to anisotropic transport. To see this, we follow Rosch [25] and solve the Boltzmann equation (BE) for scattering by impurities and spin fluctuations, which yields features not captured by the relaxation time approximation [26]. In the regime where impurity scattering dominates, we obtain the resistivity along the α ($\alpha = x, y, z$) direction:

$$\rho_{\alpha\alpha} - \rho_{\text{imp}} = \sum_{\mathbf{k}\mathbf{k}',\lambda\lambda'} \left(\Phi^{\alpha}_{\mathbf{k},\lambda} - \Phi^{\alpha}_{\mathbf{k}',\lambda'}\right)^2 \mathcal{D}^{\lambda\lambda'}_{\mathbf{k}\mathbf{k}'} \qquad (1)$$

with $\mathcal{D}^{\lambda\lambda'}_{\mathbf{k}\mathbf{k}'} \equiv f^0_{\mathbf{k}',\lambda'}\left(1 - f^0_{\mathbf{k},\lambda}\right) t^{\lambda\lambda'}_{\text{sf},\mathbf{k}\mathbf{k}'}$. Here, $\mathbf{k}$ is the electron momentum, λ is the band index, $f^0_{\mathbf{k},\lambda}$ is the Fermi-Dirac distribution function, and ρ_{imp} is the (isotropic) residual resistivity. $t^{\lambda\lambda'}_{\text{sf},\mathbf{k},\mathbf{k}'} = \sum_{i=1}^{2} g^{\lambda\lambda'}_{\text{sf},i}\, n(\omega)\, \text{Im}\chi_i(\mathbf{q},\omega)$ is the spin-fluctuations collision term, where $\omega = \varepsilon_{\lambda,\mathbf{k}} - \varepsilon_{\lambda',\mathbf{k}'}$ and $\mathbf{q} = \mathbf{k} - \mathbf{k}'$ are, respectively, the transferred energy and momentum, and $\chi_i(\mathbf{q},\omega)$ is the dynamic susceptibility associated with the ordering vector $\mathbf{Q}_i$. $g^{\lambda\lambda'}_{\text{sf},i}$ is the scattering amplitude and $\Phi^{\alpha}_{\mathbf{k},\lambda}$ is the deviation of the electron distribution function from equilibrium due to scattering by impurities only, as a consequence of an electric field applied along the α direction. It only depends on the impurity scattering potential $V^{\lambda\lambda'}_{\text{imp}}$ and on the shape of the FS (see supplementary material for more details).

The resistivity anisotropy data in $Ba(Fe_{1-x}Co_x)_2As_2$ show that the temperature-dependent contribution is smaller than the residual resistivity, particularly close to optimal doping [2]. Therefore, we can calculate $\rho_{\alpha\alpha}$ using Eq. (1), whose inputs are the band dispersions $\varepsilon_{\lambda,\mathbf{k}}$, which determine the impurity-only solution $\Phi^{\alpha}_{\mathbf{k},\lambda}$, and the dynamic susceptibilities $\chi_i(\mathbf{q},\omega)$, which determine the spin-fluctuation scattering amplitude $t^{\lambda\lambda'}_{\text{sf},\mathbf{k},\mathbf{k}'}$. In the Ising-nematic phase, the latter are:

$$\chi_i(\mathbf{q},\omega) = \frac{C_0}{r_i(\mathbf{q}+\mathbf{Q}_i) \mp \varphi - i\omega/\gamma}, \qquad (2)$$

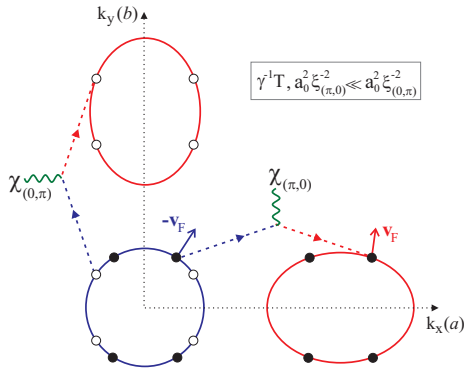

Figure 2: Electrons at the active and passive hot spots (full and empty circles, respectively) are scattered with different amplitudes by spin fluctuations associated with the $(\pi,0)$ and $(0,\pi)$ ordering vectors. The projection of the hot spots Fermi velocities (arrows) along the (a,b) axes determine the sign of the low-temperature resistivity anisotropy.

where the upper (lower) signs refers to $\mathbf{Q}_1$ ($\mathbf{Q}_2$), γ is the Landau damping parameter, and $r_i(\mathbf{q}+\mathbf{Q}_i) = a_0^2\xi^{-2} + a_0^2 q_x^2(1 \pm \eta) + a_0^2 q_y^2(1 \mp \eta) + \eta_z^2 \cos^2\left(\frac{q_z c_0}{2}\right)$. This phenomenological form follows naturally from the electronic structure of the iron pnictides [27], and is confirmed by inelastic neutron scattering experiments [28]. Here, we introduced the in-plane (out-of-plane) tetragonal lattice constant a_0 (c_0), the magnetic correlation length ξ, the in-plane momentum anisotropy η, and the out-of-plane anisotropy η_z. The temperature dependence of ξ and φ are calculated within a self-consistent mean-field approach [11, 12], yielding the equations:

$$\begin{aligned} 1 &= \frac{T}{2}\sum_{\mathbf{q},\omega_n}\left[\chi_1(\mathbf{q},\omega_n) + \chi_2(\mathbf{q},\omega_n)\right] \\ \frac{\varphi}{g} &= \frac{T}{2}\sum_{\mathbf{q},\omega_n}\left[\chi_1(\mathbf{q},\omega_n) - \chi_2(\mathbf{q},\omega_n)\right] + h_{\text{strain}}, \end{aligned} \qquad (3)$$

where ω_n are bosonic Matsubara frequencies and $h_{\text{strain}} \propto P$, with P denoting the external strain applied to detwin the samples. For $h_{\text{strain}} = 0$, Eqs. 3 have a non-trivial solution with $\varphi \neq 0$ below a temperature T_s, describing the PM-Ort (Ising-nematic) phase. This model is similar to the one used in Ref. [13], which successfully describes the lattice softening above T_s. Since $\xi_i^{-2} = \xi^{-2} \mp \varphi$, when $\varphi > 0$ (i.e. $a \parallel x$ and $b \parallel y$) the correlation length $\xi_{(\pi,0)}$ associated with the $\mathbf{Q}_1$ ordering vector lengthens while $\xi_{(0,\pi)}$, associated with $\mathbf{Q}_2$, shortens (see Fig. 1). In the figure, we present results for an AFM quantum critical point (QCP), $\xi^{-1}_{(\pi,0)}(T=0) = 0$, where fluctuations are strongest.

Substituting the susceptibilities given by (2) in the BE solution (1), we find that the low-T transport is dominated by the subset of hot spots connected by the soft ordering vector ($\mathbf{Q}_1$ for $\varphi > 0$), $\varepsilon_{\lambda,\mathbf{k}_{hs}} = \varepsilon_{\lambda',\mathbf{k}_{hs}+\mathbf{Q}_1}$, while

contributions due to $\mathbf{Q}_2 = (0, \pi)$ are negligible. It follows that

$$\rho_{\alpha\alpha} - \rho_{\rm imp} = \kappa T^{\zeta} \left(\Phi^{\alpha}_{\mathbf{k}_{hs},\lambda} - \Phi^{\alpha}_{\mathbf{k}_{hs}+\mathbf{Q}_1,\lambda'} \right)^2 \qquad (4)$$

where $\kappa > 0$ is a constant. The exponent ζ determines the T-dependence of the resistivity and is given by $\zeta = 3/2$ ($\zeta = 1$) for $T \lesssim \Lambda\, \eta_z^2$ ($T \gtrsim \Lambda\, \eta_z^2$), depending on whether the spin fluctuation spectrum is two- or three dimensional (Λ is the energy cutoff). While the experiments of Ref. [29] on $BaFe_2\,(As_{1-x}P_x)_2$ materials support $\zeta = 1$, Eq. (4) is always dominant when compared to the Fermi-liquid contribution $\rho - \rho_{\rm imp} \propto T^2$. The distinction into active and passive hot spots is not restricted to the AFM QCP and persists everywhere along the finite temperature phase boundary where soft and hard magnetic fluctuations exist. Thus, the Ising-nematic order causes an anisotropy in the spectrum of magnetic fluctuations, which induces an anisotropy in the resistivity via scattering by spin fluctuations (see Fig. 2). To determine the amplitude and sign of $\Delta\rho$, all that is left is to calculate $\Phi^{\alpha}_{\mathbf{k},\lambda}$, i.e. the solution of the BE with impurities only, which depends solely on the band dispersions $\varepsilon_{\lambda,\mathbf{k}}$.

To gain analytical insight, we introduce a simplified model with a circular hole pocket at the center of the Brillouin zone and elliptical electron pockets displaced from the center by $\mathbf{Q}_1$ and $\mathbf{Q}_2$ [14, 18], $\varepsilon_{1,\mathbf{k}} = \varepsilon_0 - k^2/2m - \mu$, $\varepsilon_{2,\mathbf{k}+\mathbf{Q}_1} = -\varepsilon_0 + k_x^2/2m_x + k_y^2/2m_y - \mu$, and $\varepsilon_{3,\mathbf{k}+\mathbf{Q}_2} = -\varepsilon_0 + k_x^2/2m_y + k_y^2/2m_x - \mu$. Here, ε_0 is the shift in the band energies, m_i are the band masses, and μ, the chemical potential. The calculation of $\Phi^{\alpha}_{\mathbf{k},\lambda}$ for this case is straightforward and is presented in the supplementary material. In particular, we find that the sign and amplitude of the anisotropy depends on the projections along k_x (parallel to a) and k_y (parallel to b) of the Fermi velocities at the hot spots $\varepsilon_{1,\mathbf{k}_{hs}} = \varepsilon_{2,\mathbf{k}_{hs}+\mathbf{Q}_1}$ (see Fig. 2). When the hot spots are close to a certain axis, there is stronger scattering by spin fluctuations when the electrons move parallel to this axis, and the resistivity is larger along this direction. Interestingly, ARPES measurements in the optimally doped $Ba\,(Fe_{1-x}Co_x)_2\,As_2$, which is close to a possible AFM QCP covered by the SC dome [30], reveal the presence of hot spots close to the k_y (b) axis [31]. According to our model, this implies $\rho_b > \rho_a$, in agreement with transport measurements [2].

To go beyond the low-T limit in Eq. (4), we numerically calculated $\Delta\rho$ from Eq. (1) for fixed band structure parameters, $m_x = 1.25m$, $m_y = 0.83m$, and $\mu = 0.05\varepsilon_0$. For the dynamic susceptibility in Eq. (2), based on previous works [13] and neutron scattering data [28], we used $g/C_0 \approx 2 \times 10^{-2}$, $\eta_z \approx 0.1$, $\eta \approx 0.5$, $\gamma \approx 350$ meV, and $C_0 \approx 1$ meV, yielding $T_s = 40$ K and $T_N = 0$. We also considered $g^{\lambda\lambda'}_{{\rm sf},i} \approx 2V^{\lambda\lambda'}_{\rm imp}$ and expressed the results in terms of the residual resistivity $\rho_{\rm imp}$.

The behavior of ρ_a and ρ_b as function of temperature is shown in Fig. 3, where we considered $\varphi > 0$, i.e. x and y parallel to a and b, respectively. In accordance to our discussion of the low-T limit, we find $\rho_b > \rho_a$ for any temperature below T_s, a behavior that lingers even when one moves away from the QCP. As expected, we also find that $\Delta\rho \sim \varphi$ close to T_s [32]. Note that the sign of $\Delta\rho$ does not depend on the sign of the in-plane momentum anisotropy η of $\chi\,(\mathbf{q}, \omega)$ in Eq. (2). As $T \to 0$, spin fluctuations are suppressed and $\Delta\rho \to 0$. In the actual data of Ref. [2], these curves are cut off by the onset of SC, which is not considered in our model.

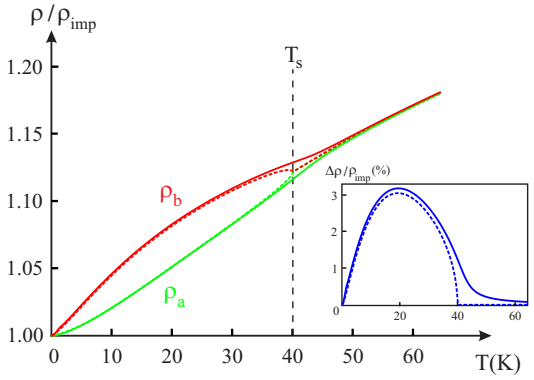

Figure 3: Temperature dependence, above the magnetic QCP, of the resistivities along a (ρ_a, green curve) and b (ρ_b, red curve), in the absence (dashed lines) and presence (full lines) of external strain. The inset shows the resistivity anisotropy $\Delta\rho = \rho_b - \rho_a$.

To make the comparison with experiments more realistic, we also included the effects of a small strain $P = 0.1$ MPa, which is applied to detwin the sample. This strain breaks the tetragonal symmetry at any temperature, and there is not a well-defined structural transition, since $\varphi \sim h^{1/\delta}_{\rm strain}$ is finite at $T_s^{\rm twin}$, where δ is the corresponding Ising critical exponent. Our calculations show that the AFM transition is practically unchanged for small strain, in agreement with the observations in Ref. [2]. If the structural transition in the twin sample is strongly first order such that $h^{1/\delta}_{\rm strain}$ is small compared to the jump of φ at $T_s^{\rm twin}$, the tail in $\Delta\rho$ above $T_s^{\rm twin}$ becomes negligible. This is the case in the parent compounds with Ba replaced by Ca or Sr, as observed by Ref. [21].

Our model also explains recent experiments that found a suppression of $\Delta\rho$ after annealing the sample [8]. As we mentioned earlier, in the ultra-clean limit the contribution of the hot spots to the resistivity is short-circuited by the other regions of the FS [24]. Since the anisotropy is governed by scattering processes near the hot spots, $\Delta\rho$ becomes smaller for cleaner samples. Our results can also be rationalized in terms of a T-dependent anisotropic dressing of the impurity scattering by spin fluctuations. Via this many-body mechanism, an s-wave scattering center acquires effectively an anisotropic cross-section, breaking the C_4 symmetry.

Finally, we discuss a general prediction of our model.

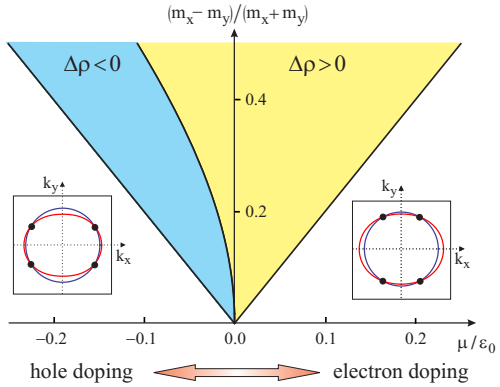

Figure 4: Sign of the low-temperature resistivity anisotropy $\Delta\rho = \rho_b - \rho_a$ as function of the ellipticity $\frac{m_x - m_y}{m_x + m_y}$ of the electron pockets and the chemical potential μ. Note the asymmetry between electron and hole doping.

When doping is introduced and the chemical potential shifts, the positions of the hot spots change accordingly. Without relying on details of $\varepsilon_{\lambda,\mathbf{k}}$, one expects that by hole-doping the samples (i.e. decreasing μ towards negative values), the area of the hole pocket increases, whereas the area of the electron pocket decreases. Consequently, active hot spots, which initially are close to the k_y (b) axis, will move towards the k_x (a) axis, and $\Delta\rho$ will eventually change its sign. This is illustrated in Fig. 4, where we present a phase diagram for the sign of $\Delta\rho$ for different values of the chemical potential μ and the ellipticity of the electron pockets $\propto m_x - m_y$, keeping the other parameters unchanged. It is interesting to note that measurements of $\Delta\rho$ in hole-doped samples $(Ba_{1-x}K_x)Fe_2As_2$ found a vanishingly small resistivity anisotropy [22], as expected near the region of the phase diagram of Fig. 4 where $\Delta\rho$ changes sign. Most interestingly, very recent data on samples with higher doping revealed a negative $\Delta\rho$, in accordance to our prediction [23].

In our approach, the resistivity anisotropy above T_N is a consequence of anisotropic scattering rates along a and b directions. Thus, optical conductivity at low frequencies is the ideal tool to verify our results. Unfortunately, as stated in Ref. [7], the experimental conditions in this temperature regime need to be refined before definite conclusions can be drawn. Yet, it is encouraging that the available data above T_N on electron-doped samples indicate a larger scattering rate along the b direction [6, 7], in agreement with our results. We stress that our model is suitable for the paramagnetic phase, where the sign of the resistivity anisotropy is determined, according to the experimental results on various compounds [2, 3, 21, 33]. Below T_N, the spin fluctuations associated with the magnetically ordered phase are naturally anisotropic, and also give rise to anisotropic scattering. Both this anisotropic scattering and the details of the anisotropic reconstruction of the FS [20, 33, 34] will govern the temperature evolution of $\Delta\rho$ below T_N.

In summary, we showed that the onset of Ising-nematic order leads to an anisotropy in the magnetic fluctuations associated with the two magnetic ground states of the iron pnictides. As a result, the same physics responsible for non-Fermi liquid behavior - the interference of scattering by spin fluctuations and impurities [25] - also gives rise to anisotropic transport properties. The latter are in agreement with several different experimental observations, such as the opposite signs of $\Delta\rho$ in electron-doped and hole-doped materials, as well as the suppression of $\Delta\rho$ upon sample annealing.

The authors thank J.-H. Chu, I. R. Fisher, R. Prozorov, and M. Tanatar for useful discussions. Research at Ames Lab was supported by the U.S. DOE, Office of BES, Materials Sciences and Engineering Division.

* Present address: Department of Physics, Columbia University, New York, New York 10027, USA.
† Present address: Karlsruhe Institute of Technology, Institute for Theory of Condensed Matter, D-76131 Karlsruhe, Germany.

[1] S. A. Kivelson, E. Fradkin, and V. J. Emery, Nature **393**, 550 (1998).
[2] J. Chu *et al.*, Science **329**, 824 (2010).
[3] M. A. Tanatar *et al.*, Phys. Rev. B **81**, 184508 (2010).
[4] M. Yi *et al.*, arXiv:1011.0050 (2010).
[5] T.-M. Chuang *et al.*, Science **327**, 181 (2010).
[6] A. Dusza *et al.*, Europhys. Lett. **93**, 37002 (2011).
[7] A. Lucarelli *et al.*, arXiv:1107.0670.
[8] M. Nakajima *et al.*, arXiv:1106.4967.
[9] Q. Si and E. Abrahams, Phys. Rev. Lett. **101**, 076401 (2008).
[10] T. Yildirim, Phys. Rev. Lett. **101**, 057010 (2008).
[11] C. Fang *et al.*, Phys. Rev. B **77,** 224509 (2008).
[12] C. Xu, M. Müller, and S. Sachdev, Phys. Rev. B **78**, 020501(R) (2008).
[13] R. M. Fernandes *et al.*, Phys. Rev. Lett. **105**, 157003 (2010).
[14] I. Eremin and A. V. Chubukov, Phys. Rev. B **81**, 024511 (2010).
[15] A. L. Wysocki, K. D. Belashchenko, and V. P. Antropov, Nat. Phys. (2011).
[16] P. Chandra, P. Coleman, and A.I. Larkin, Phys. Rev. Lett. **64**, 88 (1990).
[17] S. Nandi *et al.*, Phys. Rev. Lett. **104**, 057006 (2010).
[18] R. M. Fernandes *et al.*, Phys. Rev. B **81**, 140501(R) (2010).
[19] C. C. Chen *et al.*, Phys. Rev. B **82**, 100504 (2010).
[20] B. Valenzuela, E. Bascones, and M. J. Calderón, Phys. Rev. Lett. **105**, 207202 (2010).
[21] E. C. Blomberg *et al.*, arXiv:1101.0274.
[22] J. J. Ying *et al.*, arXiv:1012.2731.
[23] M. Tanatar and R. Prozorov, private communication.
[24] R. Hlubina and T. M. Rice, Phys. Rev. B **51**, 9253 (1995).
[25] A. Rosch, Phys. Rev. Lett. **82**, 4280 (1999).
[26] A. F. Kemper *et al.*, Phys. Rev. B **83**, 184516 (2011) .
[27] J. Zhang, R. Sknepnek, and J. Schmalian, Phys. Rev. B

82, 134527 (2010).
[28] S. O. Diallo *et al.*, Phys. Rev. B **81**, 214407 (2010); D. S. Inosov *et al.*, Nat. Phys. **6**, 178 (2010).
[29] S. Kasahara *et al.*, Phys. Rev. B **81,** 184519 (2010).
[30] J. Dai, Q. Si, J.-X. Zhu, and E. Abrahams, PNAS **106**, 4118 (2009).
[31] C. Liu *et al.*, Nat. Phys. **6**, 419 (2010).
[32] R. M. Fernandes, J. Schmalian, and H. Westfahl Jr, Phys. Rev. B **78**, 184201 (2008).
[33] H. H. Kuo *et al.*, arXiv:1103.4535.
[34] Z. P. Yin, K. Haule, and G. Kotliar, Nat. Phys. **7**, 294 (2011).